Journal of Materials Chemistry A

Accepted Manuscript

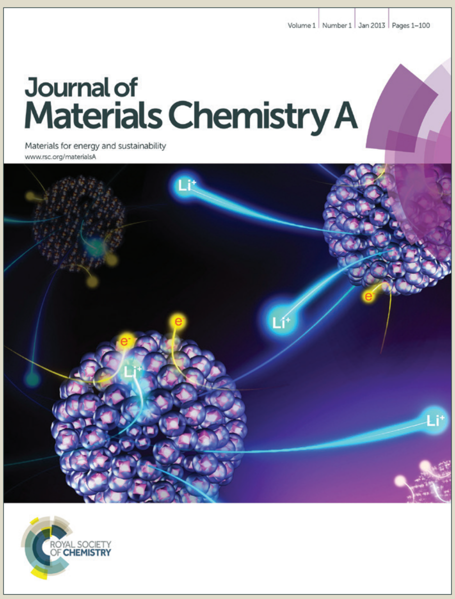

Journal Name

RSCPublishing

ARTICLE

Building Sponge-Like Robust Architectures of CNT-Graphene-Si Composites with Enhanced Rate and Cycling Performance for Lithium-Ion Batteries

Cite this: DOI: 10.1039/x0xx00000x

Received 00th January 2012,
Accepted 00th January 2012

DOI: 10.1039/x0xx00000x

www.rsc.org/

Xiaolei Wang,[a] Ge Li,[a] Fathy M. Hassan,[a] Matthew Li,[a] Kun Feng,[a] Xingcheng Xiao[b] and Zhongwei Chen[a]**

A three-dimensional robust architecture of Si-based electrode material is designed and fabricated by shielding Si nanoparticles with intertwined CNTs and graphene. Such a sponge-like unique structure enables long cycling stability of the electrode by providing void space and efficient confinement for volume change Si. In addition, the intimate contact between Si and highly conductive carbon networks improves the electrode kinetics. As a result, such a composite exhibits an outstanding capacity of 1337 mA h g^{-1} after 100 cycles at a current density of 1.0 A g^{-1}, and an improved rate performance of higher than 1000 mA h g^{-1} at a high current density of 5.0 A g^{-1}. This unique structure design endows the electrodes with high power and long cycling stability.

1. Introduction

The ever-growing demand for rechargeable lithium-ion batteries (LIBs) with high energy density, long cycle life and low cost in broad applications such as electrical vehicles and portable devices has stimulated tremendous research interest in developing novel electrode materials.[1-5] Among all the candidates for anode materials, silicon (Si) is considered as one of the most promising materials[6] owing to its high theoretical specific capacity (4200 mAh g^{-1} *vs.* 372 mAh g^{-1} of graphite) and abundance.[7] Besides, Si does not have the safety concern since there is no lithium metal dendrite formation during lithiation process.[8] However, the practical utilization of Si is still hampered by its dramatic volume variation during lithiation/delithiation process, leading to the severe pulverizaition of Si along with the solid electrolyte interphase (SEI) layer.[9, 10] Moreover the addtional SEI continually forms on the fractured silicon surfaces newly exposed to the electrolyte.[11, 12] Both the effects result in fast performance degradation of the electrode.

To overcome these two challenges, great effort has been dedicated, especially to the stabilization of Si structures and the engineering of their interfaces with electrolyte. It is generally believed that the nanostructured Si materials possess favorable mechanics for reversible morphology change,[13-15] which improves the electrochemical performance. For example, Si nanowires achieves discharge capacities of >3000 mAh g^{-1} and little fading of capacity up to 10 cycles, without mechanical damage to the Si NWs.[16] The geometry of the Si NWs and their sparse coverage are postulated to facilitate expansion/contraction.[17] Other nanostructured Si materials have also been reported, such as nanotubes,[18] hollow spheres,[19] nest-like nanospheres,[20] mesoporous sponge[21, 22] and thin films.[23] However, scalable synthesis of nanostructured Si materials that retain good long-term cycling stability in bulk electrodes of high mass loading remains a significant challenge.[21]

While the nanostructured Si materials can improve the mechanical integrity during cycling, the shielding of Si with a second phase is further considered one of the most promising tactics.[24] Various attempts have been reported on confining Si nanomaterials within rigid and spatially sealed organic or inorganic substances to stabilize the structure during the lithiation and delithation process.[25-28] For example, a life over 100 stable cycles has been demonstrated with a high loading Si anodes using pomegranate-like Si-C yolk-shell structures,[29] while a micro-sized Si-C composite consisting of interconnected Si and carbon nanoscale building blocks exhibits a reversible capacity of 1459 mA h g^{-1} after 200 cycles at 1 A g^{-1} with capacity retention of 97.8%.[30] Although such confinment significantly improves the performance, these protections are prone to disintegrate due to the huge volume expansion and contraction of interior silicon, which results in the reoccurrence of the volume change-induced problems. Therefore, it is critical to build robust and elastic substances to encapsulate Si nanoparticles.[26, 31] In addtion, maintaing the electrical connection among the nanostrucutred Si particles, conductive additives, and current collector is another challenge considering the large volume change from even stablized Si.[32, 33] A compliant structure to accomodate the volume change might be a better approah to improve the electrode integrity.[34, 35]

In this work, we report a robust structure built from flexible CNTs and elastic graphene sheets with nanosized Si particles, and demonstrate the excellent performance as anode materials for LIBs. As illustrated in **Scheme 1**, such a sponge-like architecture offers unique characteristics needed for high-power Si electrodes with long cycling stability. First, the void space created from the assembly of CNTs and graphene allows the volume expansion of Si, while the conductive carbon scaffold facilitate electron transport. Second, the elasticity and flexibility of the structure not only ensures an intimate contact between Si and conductive networks, which enables a fast electron transport and limits the SEI formation on individual Si particles, but also effectively confine the Si during volume variation and improved the electrode integrity. Furthermore, nanosized Si particles efficiently prevent fracture. Such a unique structure design endows the electrodes with high power and long cycling stability.

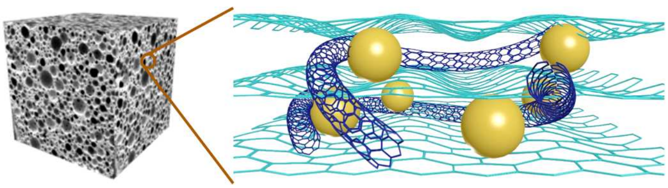

Scheme 1. Schematic of forming CNT-Graphene-Si Composites with unique 3-D architecutre.

2. Experimental

***Preparation of CNT-Graphene-Si Composites*:**

Graphene oxide (GO) was prepared from powdered flake graphite (400 mesh) by a modified Hummers method as described previously.[36] Multi-wall carbon nanotubes (CNTs) were mild-functionalized by generating carboxylic groups on their surface using a method similar to that by Gao *et al.*.[37] The CNT-graphene-Si composites were prepared by mixing those three components followed by freeze-drying process and sintering. In a typical process, a well-dispersed aqueous GO suspension (6 mg mL^{-1}, 7.5 mL) and a well-dispersed aqueous CNTs suspension (3.75 mg mL^{-1}, 8 mL) were mixed with an aqueous Si dispersion (15 mg mL^{-1}, 5 mL), forming homogeneous dispersion using probe dismembrator for 2 hr (pulse mode in ice bath). The dispersion was freeze-dried for 3 days forming a sponge-like gel before sintered under 900 ^oC in a H_2/Ar (90:10) flow for 4 hrs with a ramping rate of 2 ^oC min^{-1} from room temperature to 550 ^oC and 5 ^oC min^{-1} from 550 ^oC to 900 ^oC . The sponge-like morphology was preserved.

***Material Characterization*:**

Nitrogen sorption isotherms were measured at 77 K with a Micromeritics ASAP 2020 analyzer. Scanning electron microscopic (SEM) experiments were conducted on a LEO FESEM 1530; transmission electron microscopic (TEM) experiments were conducted on a JEOL 2010F TEM/STEM field emission microscope equipped with a large solid angle for high-X-ray throughput, scanning, scanning-transmission and a Gatan imaging filter (GIF) for energy filtered imaging from the Canadian Center for Electron Microscopy (CCEM) located at McMaster University. Raman scattering spectra were recorded on a Bruker Sentterra system (532 nm laser). Thermal Gravimetric Analysis (TGA) was conducted on TA instrument Q500. TGA testing was performed in air with a temperature range of 25 °C to 850 °C and a ramp rate of 10 °C min^{-1}.

***Electrode Fabrication*:**

A convention slurry-coating process was used to fabricate the electrodes. The active material powders and sodium salt of carboxy methyl cellulose (NaCMC) binder were mixed in a mass ratio of 90:10 without extra carbon black added and homogenized DDI water to form slurries. The homogenous slurries were coated on Cu foil substrates and dried at 100 ^oC for 12 hr under vacuum. The mass loading of active materials was controlled to be 0.7 to 0.9 mg cm^{-2}.

***Electrochemical Measurements*:**

To test electrodes, 2032-type coin cells were assembled in an argon-filled glovebox, using Celgard 2500 membrane as the separator, lithium foils as the counter electrodes, 1 M $LiPF_6$ in a 1:1 (v/v) mixture of ethylene carbonate and dimethyl carbonate with 10 wt% fluorinated ethylene carbonate (FEC) as the electrolyte. Cyclic voltammetric (CV) measurements were carried out on a VMP3 potentiostat/galvanostat (Bio-Logic LLC, Knoxville, TN) using cutoff voltages of 1.500 and 0.050 V versus Li/Li^+ at a scan rate of 0.025 mV s^{-1}. The galvanostatic charge/discharge measurements were performed on NEWARE BTS-CT3008 (Neware Technology, Ltd., Shenzhen, China) at different current densities and different cut-off voltage ranges. Electrochemical impedance spectroscopy measurement was conducted on a Princeton Applied Research VersaSTAT MC potentiostat. The Nyquist plots were recorded potentiostatically by applying an AC voltage of 10 mV amplitude in the frequency range of 0.01 to 100k Hz. All electrochemical measurements were carried out at room temperature.

3. Results and discussion

Figure 1A shows a representative scanning electron microscopic (SEM) image of as-synthesized CNT-graphene-Si composites with sponge-like architecture. It can be clearly observed that most of the surface of Si nanoparticles with average size of ~90 nm are wrapped by graphene sheets forming an effective shielding, though a very little amount of the Si nanoparticles are still exposed (**Figure 1B**). The CNTs, with the length of ~20 µm form a 3D network structure by interpenetrating through the whole composites. The composition of the composite material can be simply tuned by varying the ratio of each constituent. In this work, we focus on 66%-Si, 19%-CNT and 15%-graphene based on the thermo-gravimetric analysis result (**Figure S1**, supporting information). A high-magnification SEM image of a selected area confirms the network structure, where the CNTs, graphene and Si form intimate contact with each other (**Figure 1C and 1D**). Note that both CNT and graphene sheets are prone to form highly porous structure.[38] The composite material still possesses a 3D porous structure even after being pressed at 10 MPa (**Figure S2**). Considering the stretchable structure formed by CNTs and graphene, such a sponge-like electrode structure can well accommodate the volume variation of Si during lithiation/delithiation. In addition, the transmission electron microscopy (TEM) image in **Figure 1E** reveals that the Si particles are settled within the CNTs/graphene network structure. To further elucidate how the CNTs/graphene networks interact with Si particles, element mapping was performed using scanning transmission electron microscopy (STEM) energy-dispersive X-ray (EDS) spectroscopy technique. As shown in **Figure 1F**, the uniform dispersion of carbon element indicates the effective formation of the robust structure and the intimate interface between the Si particles and the carbon based conductive network.

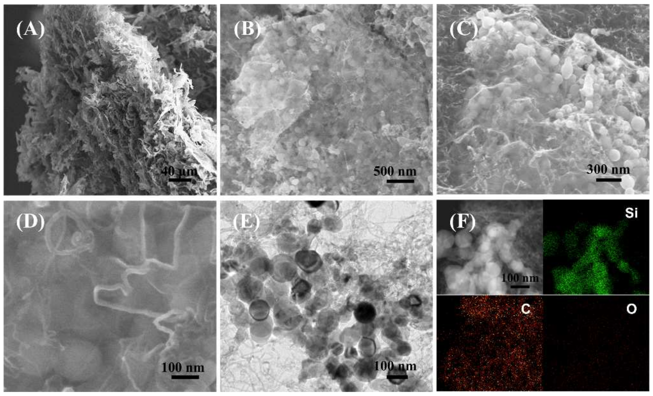

Figure 1. (A) and (B) Representative SEM images of the sponge-like architecture of the CNT-graphene-Si composites. The Si NPs are confined within CNT-graphene networks with CNTs penetrating through the whole composites. (C) and (D) High-magnification SEM image of CNT-graphene-Si composites, where the CNT backbones can be clearly observed. (E) TEM image of the composite showing Si NPs and the CNTs network. (F) Elemental mapping showing the distribution of CNT-graphene and Si NPs (up-left: spectrum image scanning, up-right: Si-K mapping, bottom-left: C-K mapping, bottom-right: O-K mapping).

Charge-storage behavior of the composites electrode was first characterized by cyclic voltammetry (CV) using coin-type half-cells with lithium foil as counter electrode, which is commonly used to characterize battery electrodes. The mass loading of active materials (including Si, CNTs and grahene) in each electrode was controlled to be ~0.7 mg cm^{-2}, in which Si comprises 60% of the total mass on each electrode. **Figure 2A** shows the first four cycles of a representative CNT-graphene-Si composite electrode at a sweep rate of 0.025 mV s^{-1} (~32 hr per cycle). Two cathodic peaks can be observed locating at 0.27 and 0.22 V, indicating the formation of different phases of $Li_{12}Si_7$ and $Li_{15}Si_4$, respectively.[39, 40] Correspondingly, two anodic peaks locating at 0.31 and 0.49 V are asscribled to the conversion of amorphous Li_xSi to Si. Both cathodic and anodic peaks become broader and stronger, which is a common characteristic for the transition from crystalline silicon to amorphous silicon due to lithiation/delithiation.[41] **Figure 2B** presents the typical galvanostatic charge/discharge curves of the composite electrodes at a voltage range of 1.5 to 0.005 V and various current densities of 0.1, 0.2, 0.5, 1.0, 2.5, and 5.0 A g^{-1}. A long flat plateau can be observed for the first discharge curve, which is consistent with the previously reported Si materials alloying with lithium to form amporphous Li_xSi.[42, 43] The electrode delivers an initial discharge capacity of 2186 mA h g^{-1} calculated by the total mass of the composite materials at a current density of 0.1 A g^{-1}, with a high initial Coulombic efficiency of 79.5%. If not mentioned, all reported capacities are based on the total mass of the composite materials. The following discharge cycles show different characteristic voltage profiles from the initial discharge curve, which is commonly attributed to the lithiation of amorphous Si. **Figure 2C** displays the corresponding rate performance of the composite electrode. The discharge capacity can be stabilized at ~1800 mA h g^{-1} at a current density of 0.1 A g^{-1} (corresponding to a discharge process of ~18 hr), while a capacity of higher than 1000 mA h g^{-1} can be retained even at a current density of 5.0 A g^{-1} (corresponding to a discharge process of ~12 min). This superior rate capability is clearly shown in **Figure 2D**. At a current density of 1.0 A g^{-1}, ~70% of the initial discharge capacity remains. Even at high current density of 5.0 A g^{-1}, the electrode is still able to preserve ~60% of its initial capacity, ~65% of its second discharge capacity at 0.1 A g^{-1}.

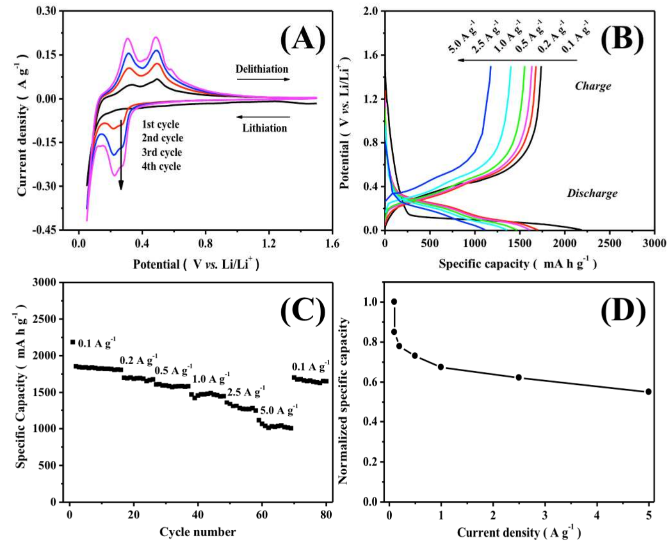

Figure 2. (A) CV plots of a representative CNT-graphene-Si composite electrode at a sweep rate of 0.025 mV s^{-1} between 1.5 and 0.05 V; (B) Galvanostatic charge/discharge curves of an composite electrode at various current densities from 0.1 to 5.0 A g^{-1} between 1.5 and 0.005 V; (C) Corresponding rate performance of the composite electrode; (D) Discharge capacity retention of the composite electrode at various current densities (the first two points represent the initial and second discharge capacities, respectively). All capacities are calculated on the total mass of the composites on the electrode.

To elucidate how such a sponge-like architecture leads to an excellent rate capability, high-resolution TEM was conducted to investigate the interface between the Si NPs and the highly conductive carbon networks. As shown in **Figure 3A**, it can be observed that a single Si NP has intimate contact with both CNTs and graphene sheets with no obvious thick SiO_2 layer observed on the surface Si NP. To further investigate the changes in chemical structure and the interface, Raman spectra was analyzed, in which the peaks positions provide information about the strain and stress in the system. As shown in **Figure 3B**, a sharp peak at ~504 cm^{-1} is clearly defined, which is right below the characteristic peak for Si at 520 cm^{-1}.[44] The peak downshift is mainly attributed to the formation of surface stress on Si NPs usually generated from different thermal expansion coefficient between Si and its coating,[45-48] which further confirms the effective shielding of Si NPs by conductive carbon networks. Apparently, the generated tensile stress in Si particles caused by carbon shielding can better balance the lithium-ion diffusion-induced compressive stress on Si surface, therefore alleviating the mechanical degradation. Additionally, another two peaks at 1352 and 1585 cm^{-1}, respectively, can be found, which correspond to the D- and G-band of carbon materials (**Figure 3B**, inset).[49] The integrated intensity ratio I_D/I_G is indicative of the degree of carbonization.[50] The small ratio of ~0.73 indicates a higher degree of carbonization. Raman mapping is used to give an insight on consistence of the materials on the electrode. **Figure 3C** presents a resolved mapping of the Si peak in a depth of 8 μm into the electrode with an area of 100×100 μm^2 marked in the optical image (**Figure S3**) from Raman spectroscopy with dispersive microscope. The bulk of the electrode is formed of Si NPs wrapped by CNT-graphene which is homogenously distributed all of the area, as evidenced by the downshift of the Si peak. The porous structure is characterized by the nitrogen adsorption-desorption isotherms. As shown in **Figure 3D**, the composite exhibits a Brunauer–Emmett–Teller (BET) surface area of only 36.0 $m^2\ g^{-1}$ and a pore diameter distribution centered below 8 nm. In contrast, the CNT-graphene architecture possesses a BET surface area of 198.9 $m^2\ g^{-1}$. This result further confirms the intimate contact between the carbon networks and the Si NPs, which is essential to facilitate the electron transportation.[51]

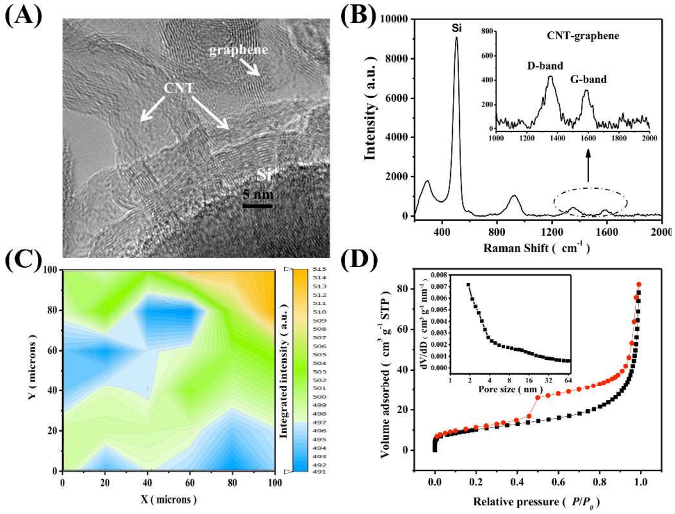

Figure 3. (A) High-resolution TEM image showing the contact between a single Si NP and the carbon networks; (B) Raman spectra of CNT-graphene-Si composite material (inset: corresponding D-band and G-band of carbon materials); (C) Raman mapping of the Si peak in a depth of 8 μm into the electrode on an area of 100×100 μm^2 marked in the optical image (Figure S2) from Raman spectroscopy with dispersive microscope; and (D) Nitrogen adsorption-desorption isotherms of CNT-graphene-Si composite material (inset: pore-size distribution of the composites).

Besides the excellent rate capability, such a robust architecture enables the electrode a significantly improved cycling stability. **Figure 4A** presents the galvanostatic charge-discharge curves of a composite electrode at different current densities for different cycles under cycling investigation. The composite electrode achieves an initial discharge capacity of 2155 mA h g^{-1} with an efficiency of 83.3%. About 78% of the theoretical capacity of Si can be obtained if calculated based on the mass of silicon in the composites. Note that the specific capacity from CNT-graphene in the same voltage window is negligible (~150 mA h g^{-1}) when compared with Si nanoparticles (**Figure S4**). The second cycle discharge capacity decreases to 1908 mA h g^{-1}, but the Coulombic efficiency increases to 95.8%. At high current density of 1.0 A g^{-1}, both the charge and discharge capacities remain stable during cycling, and a discharge capacity of 1337 mA h g^{-1} and an efficiency of 99.3% can be obtained after 100 cycles. The corresponding capacity dependence on cycle numbers is clearly shown in **Figure 4B**. The discharge capacity retention at 1.0 A g^{-1} is 80.0%, corresponding to a 0.2% capacity loss per cycle. Moreover, a very high Coulombic efficiency close to 100% is well maintained. Even cycled at low current density (0.1 A g^{-1}), an excellent cycling stability can still be obtained (**Figure S5**). To further investigate the superior cycling stability, galvanostatic charge-discharge test was carried out on another electrode at a cutting-off voltage of 1.5-0.050 V *vs.* Li/Li^+ at 0.1 A g^{-1} for 15 cycles before shifting to a higher current density of 1.0 A g^{-1} for long term cycling. As shown in **Figure 4C**, After 500 cycles, a discharge capacity of 1160 mA h g^{-1} still remains, corresponding to a 88.5% of capacity retention. By comparison, the electrode composed of 60% Si fabricated in conventional way degrades rapidly, retaining only 13.5 of its capacity after only 20 cycles at 0.1 A g^{-1}. This further proves that the Si NPs can be effectively confined within the sponge-like electrode architecture which persists against the volume expansion and contraction. To further understand the stability of the CNT-graphene-Si electrode during cycling process, electrochemical impedance spectroscopy (EIS) was conducted at frequencies from 100 kHz to 0.01 Hz. **Figure 4D** shows the Nyquist plots at different cycles (after 15 cycles at 0.1 A g^{-1} and after 75 and 200 cycles at 1.0 A g^{-1}). Each plot is composed of a semicircle at high frequency and a Warburg tail at low frequency, which represents the resistance of electrolyte and charge-transfer, and the diffusion-resistance from the electrode materials, respectively. A decrease in the semicircle can be observed during cycling, indicating an increased electrode conductivity and composite interface. Moreover, an increase in the slope of Warburg tails can also be observed due to a combined effect of the enhanced diffusion from the porosity and growth of SEI layer. Such an EIS characteristic further confirms the highly robust architecture of the electrode.

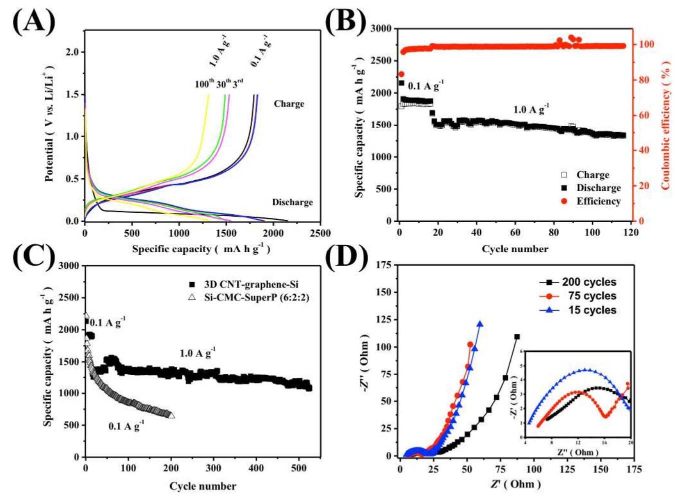

Figure 4. (A) The first three galvanostatic charge/discharge curves of a composite electrode at current densities of 0.1 and 1.0 A g^{-1} between 1.5 and 0.005 V; (B) Corresponding cycling stability of the electrode at 0.1 A g^{-1} for 16 cycles and at 1.0 A g^{-1} for 100 cycles; (C) Comparison of the cycling stability of the composite with Si-CMC-SuperP at a potential range between 1.5 to 0.050 V; and (D) Nyquist plots of the composite electrode after 15 cycles at a current density of 0.1 A g^{-1} and after 75 and 200 cycles at a current density of 1.0 A g^{-1}.

The superior cycling stability is mainly attributed to the robust CNT-graphene networks architecture (**Figure S6 and S7**), where the CNTs penetrate through the whole composite acting as an ideal scaffold with high mechanical strength.[52] Meanwhile, the soft and flexible graphene sheets provide enough toughness, which allows the electrodes to accommodate significant volume changes of Si materials. SEM and TEM images (**Figure 5**) of the electrodes after charge-discharge cycling show a well-retained network structure. Although the Si NPs cannot be clearly identified from the TEM image due to the transformation of crystalline Si into amorphous Si, they are still caged in the sponge-like carbon which persists against during expansion and contraction during lithiation/delithiation. It is well accepted that the cycling performance of Si-based electrode is strongly dependent on the mass loading of the electrode. To further investigate the advantage of robust CNT/graphene networks, a higher mass loading of 1.39 mg cm^{-2} was also applied. A capacity retention of 76.7% can be achieved at a current density of 100 mA g^{-1} for 150 cycles between 1.5 to 0.005 V (**Figure S8**).

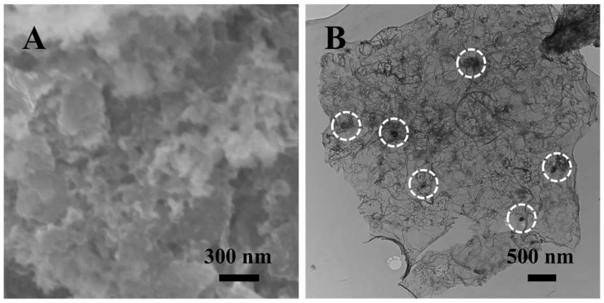

Figure 5. (A) SEM and (B) TEM images of the electrode after charge-discharge cycling for 100 cycles at the voltage range between 1.500 to 0.005 V vs. Li/Li^+. The white dashed cycles point out several places where Si NPs exist.

4. Conclusions

In summary, we have successfully developed a sponge-like robust structure for high-performance Si anode by confining Si particles in flexible and stretchable CNT-graphene networks. The resulting electrodes achieve high rate-capability and long cycling-stability, due to the highly conductive carbon-based networks, the efficient shielding of the Si surfaces, and the stretchable porous structure which is able to accommodate the Si volume variation during cycling. Such a design and fabrication endows the Si-based electrodes with both high power and long cycling stability.

Acknowledgements

This work was supported by the Natural Sciences and Engineering Research Council of Canada (NSERC), the University of Waterloo, and the Waterloo Institute for Nanotechnology. The authors also acknowledge the financial support from the Assistant Secretary for Energy Efficiency and Renewable Energy, Office of Vehicle Technologies of the U.S. Department of Energy under contract no. DE-AC02-05CH11231, subcontract no. 7056410 under the Batteries for Advanced Transportation Technologies (BATT) Program.

Notes and references

[a] *Dr. X. Wang, Dr. G. Li, F. M. Hassan, M. Li, K. Feng, Prof. Z. Chen, Department of Chemical Engineering, University of Waterloo, Waterloo, Ontario N2L3G1, Canada*
Corresponding author Tel: 1-(519)888-4567 Ext: 38664
E-mail: zhwchen@uwaterloo.ca
[b] *Dr. X. Xiao*
Chemical Sciences and Materials Systems, General Motors Global Research and Development Center, Warren, Michigan 48090, United States
Corresponding author Tel: 1-(248)912-8132
E-mail: xingcheng.xiao@gm.com

† Electronic Supplementary Information (ESI) available: [details of any supplementary information available should be included here]. See DOI: 10.1039/b000000x/

1. M. Armand and J. M. Tarascon, *Nature*, 2008, 451, 652-657.
2. J. M. Tarascon and M. Armand, *Nature*, 2001, 414, 359-367.
3. M. S. Whittingham, *MRS Bulletin*, 2008, 33, 411-419.
4. A. S. Arico, P. Bruce, B. Scrosati, J.-M. Tarascon and W. van Schalkwijk, *Nat Mater*, 2005, 4, 366-377.
5. G. H. Jeong, H.-B. Bae, D. Choi, Y. H. Kim, S. Yoon and S.-W. Kim, *The Journal of Physical Chemistry C*, 2012, 116, 23851-23857.
6. Y. Yang, H. Zhang, Y. Liu, Z.-H. Lin, S. Lee, Z. Lin, C. P. Wong and Z. L. Wang, *ACS Nano*, 2013, 7, 2808-2813.
7. M. N. Obrovac, L. Christensen, D. B. Le and J. R. Dahn, *Journal of The Electrochemical Society*, 2007, 154, A849-A855.
8. U. Kasavajjula, C. Wang and A. J. Appleby, *Journal of Power Sources*, 2007, 163, 1003-1039.
9. M. N. Obrovac and L. Christensen, *Electrochemical and Solid-State Letters*, 2004, 7, A93-A96.
10. R. Yi, F. Dai, M. L. Gordin, H. Sohn and D. Wang, *Advanced Energy Materials*, 2013, 3, 1507-1515.
11. W.-J. Zhang, *Journal of Power Sources*, 2011, 196, 13-24.
12. B. Hertzberg, A. Alexeev and G. Yushin, *Journal of the American Chemical Society*, 2010, 132, 8548-8549.
13. H. Wu and Y. Cui, *Nano Today*, 2012, 7, 414-429.
14. P. D. Lund, G. Hashmi, Y. Ma, J. Patakangas and Y. Jing, *Microelectronic Engineering*, 2014, 126, 49-53.
15. N. Ali and P. Lund, *International Journal of Energy Research*, 2014, 38, 415-417.
16. C. K. Chan, H. Peng, G. Liu, K. McIlwrath, X. F. Zhang, R. A. Huggins and Y. Cui, *Nat Nano*, 2008, 3, 31-35.
17. T. Song, J. Xia, J.-H. Lee, D. H. Lee, M.-S. Kwon, J.-M. Choi, J. Wu, S. K. Doo, H. Chang, W. I. Park, D. S. Zang, H. Kim, Y. Huang, K.-C. Hwang, J. A. Rogers and U. Paik, *Nano Letters*, 2010, 10, 1710-1716.
18. M.-H. Park, M. G. Kim, J. Joo, K. Kim, J. Kim, S. Ahn, Y. Cui and J. Cho, *Nano Letters*, 2009, 9, 3844-3847.
19. Y. Yao, M. T. McDowell, I. Ryu, H. Wu, N. Liu, L. Hu, W. D. Nix and Y. Cui, *Nano Letters*, 2011, 11, 2949-2954.
20. H. Ma, F. Cheng, J. Y. Chen, J. Z. Zhao, C. S. Li, Z. L. Tao and J. Liang, *Advanced Materials*, 2007, 19, 4067-4070.
21. X. Li, M. Gu, S. Hu, R. Kennard, P. Yan, X. Chen, C. Wang, M. J. Sailor, J.-G. Zhang and J. Liu, *Nat Commun*, 2014, 5.
22. H. Kim, B. Han, J. Choo and J. Cho, *Angewandte Chemie*, 2008, 120, 10305-10308.
23. J. P. Maranchi, A. F. Hepp and P. N. Kumta, *Electrochemical and Solid-State Letters*, 2003, 6, A198-A201.
24. B. Wang, X. Li, X. Zhang, B. Luo, M. Jin, M. Liang, S. A. Dayeh, S. T. Picraux and L. Zhi, *ACS Nano*, 2013, 7, 1437-1445.
25. H. Wu, G. Zheng, N. Liu, T. J. Carney, Y. Yang and Y. Cui, *Nano Letters*, 2012, 12, 904-909.
26. Z. Chen, J. W. F. To, C. Wang, Z. Lu, N. Liu, A. Chortos, L. Pan, F. Wei, Y. Cui and Z. Bao, *Advanced Energy Materials*, 2014, DOI: 10.1002/aenm.201400207, n/a-n/a.
27. F. M. Hassan, V. Chabot, A. R. Elsayed, X. Xiao and Z. Chen, *Nano Letters*, 2013, 14, 277-283.
28. R. Yi, J. Zai, F. Dai, M. L. Gordin and D. Wang, *Nano Energy*, 2014, 6, 211-218.
29. N. Liu, Z. Lu, J. Zhao, M. T. McDowell, H.-W. Lee, W. Zhao and Y. Cui, *Nat Nano*, 2014, 9, 187-192.
30. R. Yi, F. Dai, M. L. Gordin, S. Chen and D. Wang, *Advanced Energy Materials*, 2013, 3, 295-300.
31. C. Wang, H. Wu, Z. Chen, M. T. McDowell, Y. Cui and Z. Bao, *Nat Chem*, 2013, 5, 1042-1048.
32. X. Li, P. Meduri, X. Chen, W. Qi, M. H. Engelhard, W. Xu, F. Ding, J. Xiao, W. Wang, C. Wang, J.-G. Zhang and J. Liu, *Journal of Materials Chemistry*, 2012, 22, 11014-11017.
33. J. Xiao, W. Xu, D. Wang, D. Choi, W. Wang, X. Li, G. L. Graff, J. Liu and J.-G. Zhang, *Journal of The Electrochemical Society*, 2010, 157, A1047-A1051.

34. D. Wang, X. Li, J. Wang, J. Yang, D. Geng, R. Li, M. Cai, T.-K. Sham and X. Sun, *The Journal of Physical Chemistry C*, 2012, 116, 22149-22156.
35. W. J. Lee, T. H. Hwang, J. O. Hwang, H. W. Kim, J. Lim, H. Y. Jeong, J. Shim, T. H. Han, J. Y. Kim, J. W. Choi and S. O. Kim, *Energy & Environmental Science*, 2014, 7, 621-626.
36. D. Li, M. B. Muller, S. Gilje, R. B. Kaner and G. G. Wallace, *Nat Nano*, 2008, 3, 101-105.
37. C. Gao, C. D. Vo, Y. Z. Jin, W. Li and S. P. Armes, *Macromolecules*, 2005, 38, 8634-8648.
38. J. Yan, T. Wei, Z. Fan, W. Qian, M. Zhang, X. Shen and F. Wei, *Journal of Power Sources*, 2010, 195, 3041-3045.
39. B. Liu, P. Soares, C. Checkles, Y. Zhao and G. Yu, *Nano Letters*, 2013, 13, 3414-3419.
40. B. Key, M. Morcrette, J.-M. Tarascon and C. P. Grey, *Journal of the American Chemical Society*, 2010, 133, 503-512.
41. H. Wu, G. Yu, L. Pan, N. Liu, M. T. McDowell, Z. Bao and Y. Cui, *Nat Commun*, 2013, 4.
42. A. Magasinski, P. Dixon, B. Hertzberg, A. Kvit, J. Ayala and G. Yushin, *Nat Mater*, 2010, 9, 353-358.
43. S. W. Lee, M. T. McDowell, L. A. Berla, W. D. Nix and Y. Cui, *Proceedings of the National Academy of Sciences*, 2012, 109, 4080-4085.
44. J. Zi, H. Buscher, C. Falter, W. Ludwig, K. Zhang and X. Xie, *Applied Physics Letters*, 1996, 69, 200-202.
45. L. Khriachtchev, O. Kilpela, S. Karirinne, J. Keranen and T. Lepisto, *Applied Physics Letters*, 2001, 78, 323-325.
46. L. Khriachtchev, M. Rasanen, S. Novikov and L. Pavesi, *Applied Physics Letters*, 2004, 85, 1511-1513.
47. D. Nesheva, C. Raptis, A. Perakis, I. Bineva, Z. Aneva, Z. Levi, S. Alexandrova and H. Hofmeister, *Journal of Applied Physics*, 2002, 92, 4678-4683.
48. W. Zhang, S. Zhang, Y. Liu and T. Chen, *Journal of Crystal Growth*, 2009, 311, 1296-1301.
49. H. Kim and J. Cho, *Nano Letters*, 2008, 8, 3688-3691.
50. F. Tuinstra and J. L. Koenig, *The Journal of Chemical Physics*, 1970, 53, 1126-1130.
51. B. Zhang, Q. B. Zheng, Z. D. Huang, S. W. Oh and J. K. Kim, *Carbon*, 2011, 49, 4524-4534.
52. W. Wang, S. Guo, M. Penchev, I. Ruiz, K. N. Bozhilov, D. Yan, M. Ozkan and C. S. Ozkan, *Nano Energy*, 2013, 2, 294-303.

Journal Name RSCPublishing

ARTICLE

Building Sponge-Like Robust Architectures of CNT-Graphene-Si Composites with Enhanced Rate and Cycling Performance for Lithium-Ion Batteries

Xiaolei Wang,[a] *Ge Li,*[a] *Fathy M. Hassan,*[a] *Matthew Li,*[a] *Kun Feng,*[a] *Xingcheng Xiao*[b]* *and Zhongwei Chen*[a]*

High-performance robust CNT-graphene-Si composites are designed as anode materials with enhanced rate capability and excellent cycling stability for lithium-ion batteries. Such an improvement is mainly attributed to the robust sponge-like architecture, which holds its grate promise in future practical applications.

Keyword: silicon anode; robust structure; lithium-ion battery; long cycling stability; carbon nanotube; graphene